Whole-body PET parametric imaging employing direct 4D nested reconstruction and a generalized non-linear Patlak model

Nicolas A. Karakatsanis*[a], Arman Rahmim*[a,b]
[a]Dpt of Radiology, School of Medicine, Johns Hopkins University, 601 N Caroline St, Baltimore, MD, USA 21285; [b]Dpt of Elec. and Computer Eng., Johns Hopkins University, 3400 N Charles St, Barton 105, Baltimore, MD, 21218

ABSTRACT

Graphical analysis is employed in the research setting to provide quantitative estimation of PET tracer kinetics from dynamic images at a single bed. Recently, we proposed a multi-bed dynamic acquisition framework enabling clinically feasible whole-body parametric PET imaging by employing post-reconstruction parameter estimation. In addition, by incorporating linear Patlak modeling within the system matrix, we enabled direct 4D reconstruction in order to effectively circumvent noise amplification in dynamic whole-body imaging. However, direct 4D Patlak reconstruction exhibits a relatively slow convergence due to the presence of non-sparse spatial correlations in temporal kinetic analysis. In addition, the standard Patlak model does not account for reversible uptake, thus underestimating the influx rate K_i. We have developed a novel whole-body PET parametric reconstruction framework in the STIR platform, a widely employed open-source reconstruction toolkit, a) enabling accelerated convergence of direct 4D multi-bed reconstruction, by employing a nested algorithm to decouple the temporal parameter estimation from the spatial image update process, and b) enhancing the quantitative performance particularly in regions with reversible uptake, by pursuing a non-linear generalized Patlak 4D nested reconstruction algorithm.
A set of published kinetic parameters and the XCAT phantom were employed for the simulation of dynamic multi-bed acquisitions. Quantitative analysis on the K_i images demonstrated considerable acceleration in the convergence of the nested 4D whole-body Patlak algorithm. In addition, our simulated and patient whole-body data in the post-reconstruction domain indicated the quantitative benefits of our extended generalized Patlak 4D nested reconstruction for tumor diagnosis and treatment response monitoring.

Keywords: whole-body, PET, reconstruction, parametric, Patlak, generalized, direct, 4D, nested

1. INTRODUCTION

Dynamic PET enables quantitative parametric imaging (e.g. FDG uptake rate constant K_i), and has witnessed continued interest in the context of single-bed acquisition. On the other hand, single-frame SUV PET imaging is routinely invoked in the context of multi-bed acquisition[1]. Previously, we have proposed[2,3] a scanning framework enabling clinically feasible whole-body parametric PET imaging, thus combining the benefits of multi-bed acquisition and estimation of quantitative tracer kinetic parameters from dynamic scans. This protocol is comprised of a short dynamic scan over the cardiac bed position right after administration of tracer (first phase) to measure the early section of the tracer concentration in the blood, followed by a dynamic series of whole-body scans to capture the later part of the time activity curves at every voxel over multiple beds (second phase, figure 1). The methods presented here have been designed for the whole-body protocols, however they can also be applied to conventional single-bed dynamic studies.

The standard Patlak linear graphical analysis[4] was selected as a robust approach to model the PET tracer kinetics on a voxel-basis to produce whole-body parametric images. Typically, the dynamic PET images are first reconstructed individually from the dynamically acquired PET projection data, followed by a post-reconstruction Patlak analysis to produce the parametric images. This procedure, commonly referred to as indirect or post-reconstruction parametric imaging, requires the modeling of the noise distribution in the dynamic images, which can be a challenging task as the image noise is spatially variant, thus resulting in noise enhancement in the parametric image space.

*nkaraka2@jhmi.edu; arahmim1@jhmi.edu; phone 1 410 614-1738; www.jhu.edu/rahmim

Medical Imaging 2014: Physics of Medical Imaging, edited by Bruce R. Whiting, Christoph Hoeschen, Despina Kontos,
Proc. of SPIE Vol. 9033, 90330Y · © 2014 SPIE · CCC code: 1605-7422/14/$18 · doi: 10.1117/12.2043918

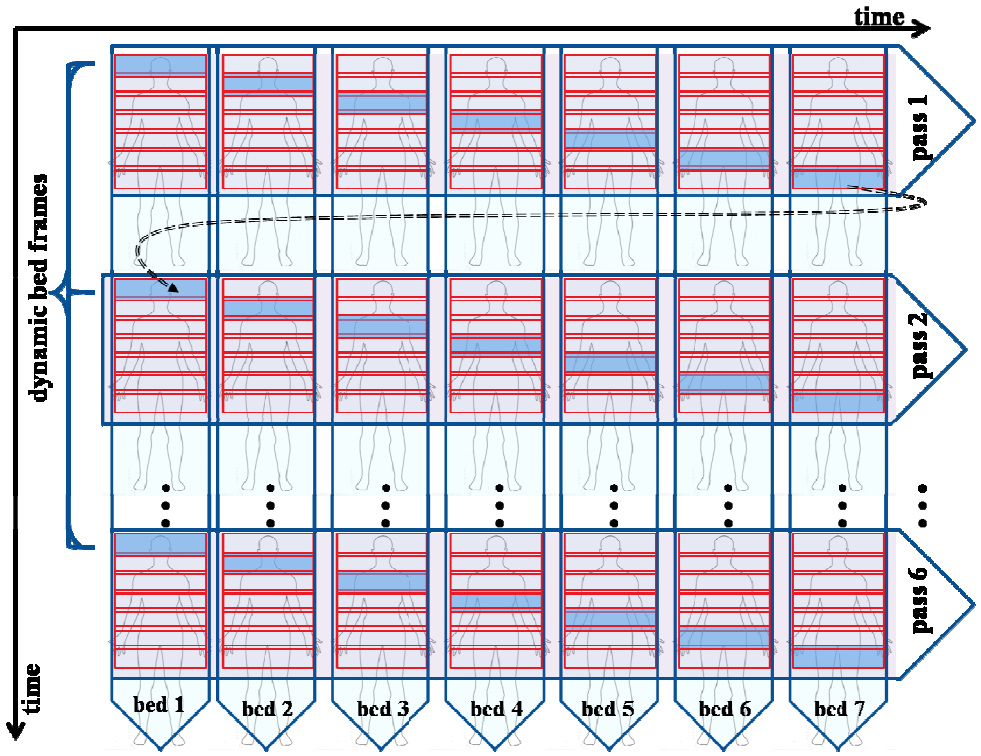

Figure 1. Illustration of an example of a dynamic bed frame sequence of the second phase of our proposed whole-body dynamic PET acquisition protocol. The particular example consists of 6 whole body passes, each comprised of 7 beds and has been optimized for human whole-body dynamic PET studies conducted with GE Discovery RX PET/CT scanner. Due to the multi-bed extension of the dynamic scan, time gaps in the acquisition are introduced between subsequent dynamic frames of each bed.

1.1 Nested direct 4D vs. indirect reconstruction

On the other hand, four-dimensional (4D) parametric reconstruction is capable of directly estimating parametric images from the dynamic raw projection data, where the measured counts can be considered as independent random variables following the Poisson distribution[5]. As a result, direct 4D reconstruction can more accurately model the noise, and thus, more efficiently compensate for its propagation to the parameter estimation process[6]. Recently, we implemented a direct 4D maximum-likelihood expectation-maximization (ML-EM) parametric reconstruction algorithm for whole-body linear Patlak modeling[8] within the STIR open-source reconstruction toolkit[7], extending a 4D implementation for continuous single-bed imaging available in STIR[9].

Nevertheless, conventional direct 4D reconstruction algorithms involve large and sparse system response matrices, to include both spatial and temporal correlations within the same update process, resulting in the propagation of the spatial correlations into the temporal parameter estimation process and vice versa. Consequently, the convergence speed of the parametric image updates decelerates in comparison to indirect methods, particularly when the temporal basis functions are correlated, e.g. linear Patlak model[5,10]. Therefore, in the current study we propose implementing the direct 4D Patlak reconstruction by utilizing the optimization transfer principle and a resulting nested version of the conventional 4D MLEM algorithm to efficiently separate the temporal estimation process from the spatial image update thus decoupling the corresponding temporal and spatial correlations[17,18].

1.2 Need for non-linear generalized Patlak model

Standard linear Patlak analysis directly estimates the uptake rate constant K_i and blood distribution volume V by assuming a two-compartment kinetic model with an irreversible compartment, a commonly invoked model for organs

and tumors exhibiting FDG uptake in PET human studies[4]. However a considerable number of studies report kinetic parameter data suggesting a certain degree of reversibility[11-13]. The linear Patlak model assumes no reversible uptake and can be seen[14-16] to underestimate K_i to account for lack of appropriate modeling of reversibility, thus compromising quantitative accuracy. We propose a novel generalized PET imaging reconstruction framework to allow for truly quantitative whole body parametric imaging including in regions exhibiting reversibility. For this purpose, an extended non-linear Patlak graphical analysis[4] is presented, equipped with an additional net efflux rate constant k_{loss} to properly account for reversibility. In addition, we incorporate this non-linear generalized Patlak model within a 4D reconstruction nested framework to a) limit the enhanced noise levels involved in non-linear kinetic modeling and b) benefit from the fast convergence properties of nested MLEM algorithms.

2. METHODOLOGY

2.1 Linear Patlak graphical analysis

The linear Patlak model utilizes dynamic PET image data and the time course of blood plasma tracer concentration (input function) to estimate the kinetic macro-parameters K_i and V at each voxel[4]:

$$\frac{C(t)}{C_P(t)} = K_{\mathrm{i}} \frac{\int_0^t C_P(\tau)d\tau}{C_P(t)} + V \Rightarrow C(t) = K_{\mathrm{i}} \int_0^t C_P(\tau)d\tau + VC_P(t) = K_{\mathrm{i}} \otimes C_P(t) + VC_P(t)\ ,\ t > t^* \tag{1}$$

where $\otimes$ denotes the temporal convolution operation, $C(t)$ is the measured time activity curve (TAC) at each voxel, $C_P(t)$ is the input function estimated either from an image region-of-interest (ROI) or from blood sampling and t^* is the time after which relative kinetic equilibrium between the blood and the reversible compartment is attained. Eq. 1 is based on the following definition[4] for $\mathrm{K_i}$: $K_{\mathrm{i}} = C_0(\infty) \Big/ \int_0^\infty C_p(\tau)d\tau$, where $C_0(\infty)$ denotes the tracer concentration left in the system at infinite time if uptake is irreversible.

2.2 Nested direct 4D MLEM Patlak reconstruction

Letting $\mathbf{Y} = \bar{\mathbf{P}}\mathbf{M}$, where $\mathbf{Y} = \left[y^1 \cdots y^N \right]^T$ are the N dynamic projection data, $\mathbf{M} = [\mathbf{K}, \mathbf{V}]^T$ are the parametric images of slope and intercept and $\bar{\mathbf{P}}$ is the spatio-temporal system matrix:

$$\bar{\mathbf{P}} = \begin{bmatrix} S_P(1)\mathbf{P} & \mathrm{C}_P(1)\mathbf{P} \\ \vdots & \vdots \\ S_P(N)\mathbf{P} & \mathrm{C}_P(N)\mathbf{P} \end{bmatrix} = \mathbf{B} \oplus \mathbf{P}\ ,\ \mathbf{y}^n = \mathbf{P}\mathbf{x}^n\ ,\ \mathbf{B} = \begin{bmatrix} S_P(1) & \mathrm{C}_P(1) \\ \vdots & \vdots \\ S_P(N) & \mathrm{C}_P(N) \end{bmatrix} \tag{2}$$

where $\oplus$ denotes the Kronecker product and $C_P(n) = C_p(t_n), S_P(n) = \int_0^{t_n} C_p(\tau)\mathrm{d}\tau$ are the plasma activity and its integral from injection to frame time t_n. According to Patlak eq. (1), for the j^{th} voxel of n^{th} image:

$$x_j^n = K_j S_P(n) + V_j C_P(n)\ \ ,\ y^n(K,V) = Px^n = P\left(\mathbf{K}S_P(n) + \mathbf{V}C_P(n)\right) \tag{3}$$

where $\mathbf{K}$ and $\mathbf{V}$ denote the K_i and V parametric images respectively. Then the two 4D MLEM update eq. follows:

$$\mathbf{K}_{new} = \frac{\mathbf{K}_{old}}{P^T\mathbf{1}\sum_{n=1}^N S_P(N)} \sum_{n=1}^N S_P(n)\mathbf{P}^T \left[\frac{\mathbf{y}^n}{\mathbf{y}^n(\mathbf{K}_{old}, \mathbf{V}_{old})} \right],\ \mathbf{V}_{new} = \frac{\mathbf{V}_{old}}{P^T\mathbf{1}\sum_{n=1}^N C_P(N)} \sum_{n=1}^N C_P(n)\mathbf{P}^T \left[\frac{\mathbf{y}^n}{\mathbf{y}^n(\mathbf{K}_{old}, \mathbf{V}_{old})} \right] \tag{4}$$

The nested 4D Patlak reconstruction algorithm initially calculates a dynamic image $\mathbf{x}^n$ utilizing system matrix **P**, followed by a nested MLEM loop of updates of the kinetic parameter images employing the kinetic model matrix **B** and using the previously estimated dynamic image as reference data[17,18]**:**

$$\hat{\mathbf{x}}^n = \frac{\mathbf{x}^n(\mathbf{K}_{old}, \mathbf{V}_{old})}{P^T\mathbf{1}} \mathbf{P}^T \left[\frac{\mathbf{y}^n}{\mathbf{y}^n(\mathbf{K}_{old}, \mathbf{V}_{old})} \right], \mathbf{K}_{new} = \frac{\mathbf{K}_{old}}{\sum_{n=1}^{N} S_P(N)} \sum_{n=1}^{N} S_P(n) \left[\frac{\hat{\mathbf{x}}^n}{\mathbf{x}^n(\mathbf{K}_{old}, \mathbf{V}_{old})} \right], \mathbf{V}_{new} = \frac{\mathbf{V}_{old}}{\sum_{n=1}^{N} C_P(N)} \sum_{n=1}^{N} C_P(n) \left[\frac{\hat{\mathbf{x}}^n}{\mathbf{x}^n(\mathbf{K}_{old}, \mathbf{V}_{old})} \right] \quad (5)$$

A single full MLEM iteration of the nested 4D algorithm consists of a single outer update of the dynamic image $\mathbf{x}^n$ and multiple nested updates of the parametric images **K** and **V**, based on the estimated dynamic image. The outer loop performs the computationally expensive forward- and back-projection operations between the dynamic image and projection space, while the nested loop utilizes a considerably smaller size matrix **B** to forward- and back-project much faster between the parametric and the temporal image space. As a result, the faster temporal parameter estimation is efficiently decoupled from the slower spatial image update process thus accelerating convergence rate.

2.3 Non-linear generalized Patlak graphical analysis and simplified Patlak kinetic models (SPKMs)

Later, retaining the same definition for K_i, Patlak and Blasberg[4] introduced an extended Patlak model to account for mildly reversible kinetics. A k_{loss} kinetic parameter was introduced to describe the net rate constant for metabolized tracer loss to the blood plasma. By assuming $k_{loss} << K_i$ the following non-linear Patlak equation can be obtained:

$$\frac{C(t)}{C_p(t)} = K_i \frac{\int_0^t e^{-k_{loss}(t-\tau)} C_p(\tau) d\tau}{C_p(t)} + V \Rightarrow C(t) = K_i \int_0^t e^{-k_{loss}(t-\tau)} C_p(\tau) d\tau + V C_p(t) = \left(K_i e^{-k_{loss} t} \right) \otimes C_p(t) + V C_p(t), \; t > t^*, \; k_{loss} << K_i \quad (6)$$

The Patlak linear model assumes a two- compartment kinetic model involving 3 rate constants (K_1, k_2 and k_3) with the second compartment considered irreversible (k_4=0) (Figure 2, top left). Linear Patlak eq. 1 effectively simplifies the two-compartmental model into a single-compartment irreversible model for $t > t^*$ (Figure 2, top right) involving a single rate constant K_i. In this context, K_i can be considered as the impulse response function of the Simplified Patlak Kinetic Model for irreversible kinetics (SPKM1).

On the other hand, the non-linear Patlak model assumes a two-compartment model involving a non-zero k_4 parameter (Figure 1, bottom left). Similarly, by restructuring eq. 6, we see that the non-linear Patlak model effectively reduces to a reversible single-compartment model (Figure 2, bottom right). Thus, we consider $K_i e^{-k_{loss} t}$ as the impulse response function of the Simplified Patlak Kinetic Model for reversible kinetics (SPKM2).

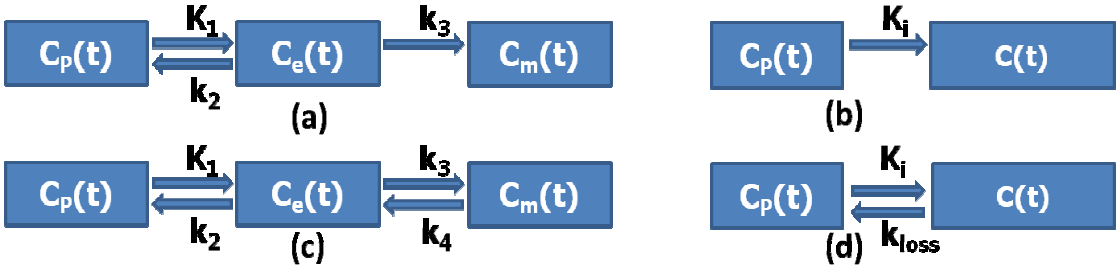

Figure 2: (left) Two-compartment kinetic models (a) without and (c) with reversibility for FDG tracer and (right) the equivalent single-compartment (b) SPKM1 and (d) SPKM2 models under Patlak graphical analysis assumptions.

2.4 Direct 4D nested incorporating the non-linear generalized Patlak graphical analysis

For the generalized non-linear Patlak model let ***K*** and $\boldsymbol{k}_{loss}$ denote the respective K_i and k_{loss} parametric images. Then, if $\mathbf{h}_0\left(K_i^j, k_{loss}^j, \mathbf{t}\right) = K_i^j \exp\left(-k_{loss}^j \mathbf{t}\right)$ is the impulse response time vector of the SPKM2 model, a TAC at voxel j

$\mathbf{x}_j = \{x_j^n\}_{n=1}^N$ can be given by: $\mathbf{x}_j\left(K_i^j, k_{loss}^j, V^j\right) = \mathbf{h}_0\left(K_i^j, k_{loss}^j, \mathbf{t}\right) \otimes \mathbf{C_p}(\mathbf{t}) + V^j \mathbf{C_p}(\mathbf{t})$. By approximating the convolution with a summation over n_k finely sampled time convolution points t'_k, we can describe $\mathbf{x}_j$ as follows:

$$\mathbf{x}_j\left(K_i^j, k_{loss}^j, V^j\right) = \mathbf{\Theta h}^j, \quad \mathbf{\Theta} = \begin{bmatrix} C_p(t_1 - t'_1) & \cdots & C_p\left(t_1 - t'_{n_k}\right) & C_p(t_1) \\ \vdots & & \vdots & \vdots \\ C_p(t_n - t'_1) & \cdots & C_p\left(t_n - t'_{n_k}\right) & C_p(t_n) \end{bmatrix}, \quad \mathbf{h}^j = \begin{bmatrix} K_i^j e^{-k_{loss}^j t'_1} \\ \vdots \\ K_i^j e^{-k_{loss}^j t'_{n_k}} \\ V^j \end{bmatrix} \tag{7}$$

Then, a nested generalized Patlak algorithm utilizing the relationship above can be described. The new algorithm will have the same outer loop update equation as before. The nested update eq. and the log-likelihood follows:

$$\hat{h}_j^k = \frac{h_j^k\left(K_{i\,\text{old}}^j, k_{loss\,\text{old}}^j, V_{\text{old}}^j\right)}{\sum_{n=1}^N \Theta_{n,k}} \sum_{n=1}^N \Theta_{n,k} \left[\frac{\hat{x}_j^n}{x_j^n\left(K_{i\,\text{old}}^j, k_{loss\,\text{old}}^j, V_{\text{old}}^j\right)} \right], \quad \boldsymbol{\theta}_{new}^j = \arg\max_{\boldsymbol{\theta}^j} \sum_{k=1}^{n_k} \hat{h}_j^k \log h_j^k\left(\boldsymbol{\theta}^j\right) - h_j^k\left(\boldsymbol{\theta}^j\right), \; \boldsymbol{\theta}^j = \left[K_i^j, k_{loss}^j, V^j\right] \tag{8}$$

The **V** parametric image is included as a distinct element in $\hat{\mathbf{h}}$ and thus is updated in eq. (8). The analytical solution[18,19] for **K** and $\mathbf{k}_{\text{loss}}$ images optimizing the log-likelihood for each j^{th} voxel above is provided as follows:

$$k_{loss\,new}^j = \text{S}^{-1}\left\{ \frac{\sum_{k=1}^{n_k} t'_k \hat{h}_k^j}{\sum_{k=1}^{n_k} \hat{h}_k^j} \right\}, \; K_{i\,\text{new}}^j = \frac{\sum_{k=1}^{n_k} \hat{h}_k^j}{\sum_{k=1}^{n_k} e^{-k_{loss\,\text{new}}^j t'_k}}, \; \text{S}\left(k_{loss}\right) = \frac{\sum_{k=1}^{n_k} t'_k e^{-k_{loss}^j t'_k}}{\sum_{k=1}^{n_k} e^{-k_{loss}^j t'_k}}, \; \text{S}^{-1} \equiv \text{inverse function of S} \tag{9}$$

While ordinary least squares (OLS) regression can be employed for the standard linear Patak parameters estimation, for the non-linear generalized Patlak model we propose a Basis Function Method (BFM)[20].

Initially a global range of q (e.g. 1000) discrete candidate k_{loss} values (e.g. $[10^{-4}, 10^{-1}]$) is determined from eq. 10 using a collection of k-values reported in literature[11-13]. Then q basis functions, each representing a candidate k_{loss} value, are constructed to linearize the problem (eq. 11):

$$C(t) = K_i B_\omega(t) + V C_p(t), \; t > t^* \;, \; B_\omega(t) = C_P \otimes e^{-k_{loss}(\omega) t} \;, \omega = 1 \ldots q \tag{10}$$

Subsequently, for each of the q basis functions associated with a particular $k_{loss}(\omega)$ value, OLS regression is applied to Eq. 8 to estimate $K_i(\omega)$ and $V(\omega)$ parameters and calculate the corresponding residual sum of squares $RSS(\omega)$. The set of estimated parameters ($K_i(\omega)$, $k_{loss}(\omega)$,$V(\omega)$) yielding the minimum $RSS(\omega)$ is finally selected.

3. DATA AND TOOLS

In the current study we generated both simulated and human clinical PET dynamic data. For the quantitative evaluation of the direct 4D parametric image reconstruction methods we employed realistic simulated data, while the clinical patient data were used to demonstrate the potential of the generalized Patlak kinetic model on the kinetic analysis of dynamic whole body clinical images and the indirect estimation of the respective parametric images.

Initially, a set of realistic time activity curves (TACs) were constructed for various characteristic regions/organs of the human body by employing a set of kinetic micro-parameters as obtained from an extensive literature review (Table 1) and assuming the complete 2-compartment kinetic model of figure 2c. Then, a dynamic series of noise-free phantom images were carefully generated by assigning the previous TACs to the respective defined regions of the advanced voxelized XCAT human torso phantom at the corresponding time frames of our proposed protocol (figure 1). Later, analytic simulations were conducted with the appropriate levels of Poisson noise corresponding to the short time frame

lengths of the multi-bed dynamic protocol and the degree of attenuation in the human torso regions as modeled by the XCAT phantom. Finally, the resulting noisy dynamic PET projection data were reconstructed in either 3D or 4D mode using our extended STIR software libraries to produce reconstructed PET and Patlak parametric images respectively. While, in the case of direct 4D reconstruction, the parametric images were estimated directly from the sinograms, for the 3D reconstructions, the resulting dynamic PET images were further analyzed kinetically, assuming the two presented Patlak models, to indirectly estimate the Patlak parametric images as well.

Table 1. Published FDG kinetic parameter values employed to generate realistic XCAT dynamic images for simulated dynamic multi-bed acquisitions

Regions	$\mathbf{K_1}$	$\mathbf{k_2}$	$\mathbf{k_3}$	$\mathbf{k_4}$	$\mathbf{V_B}$
Normal Liver	0.864	0.981	0.005	0.016	-
Liver Tumor	0.243	0.78	0.1	0	-
Normal Lung	0.108	0.735	0.016	0.013	0.017
Lung Tumor	0.044	0.231	1.149	0.259	-
Myocardium	0.6	1.2	0.1	0.001	-

4. RESULTS AND DISCUSSION

In Figure 3 the K_i parametric images are presented before and after application of spatial smoothing (Gaussian FWHM of 2mm) as produced by the conventional as well as the nested version of direct 4D linear Patlak reconstructions. For each case, a set of images are illustrated for various number of iterations. The set of parametric images corresponding to the nested 4D Patlak reconstruction achieves convergence faster, i.e. in less computation time, and also at earlier iterations where the noise levels are low to moderate. Thus the nested whole-body Patlak provides a more clinically feasible solution for enhanced tumor diagnosis in faster times and with higher contrast-to-noise (CNR) levels.

Moreover in figure (4a) we visually demonstrate in the post-reconstruction domain the advantage of generalized Patlak parametric imaging both for simulated noise-free and noisy activity distributions as well as for two clinical patient studies. Furthermore, the quantitative analysis (fig. 4b) in the simulated liver tumor confirms the superior convergence and overall better tumor CNR performance with nested 4D Patlak methods. Finally, figure (4c) presents the Patlak plots for noise-free and noisy ROIs. It becomes evident that the extended Patlak model can provide better quantitative K_i estimates than standard Patlak provided the noise is sufficiently modeled.

The results of the previous paragraph (figure 4) clearly suggest the potential of the application of generalized Patlak model in whole-body parametric imaging both for simulated and clinical data. However, these results are only based on the indirect estimation of the parametric images from the 3D reconstructed dynamic PET images. Therefore, our next step was to quantitatively also evaluate our proposed non-linear generalized Patlak 4D reconstruction methods (nested and non-nested) in order to compare their performance against the linear standard Patlak 4D algorithms. In Figure 5, the lung SNR is plotted against the number of ML-EM iterations (i.e. a single subset was used) for the non-nested (POSMAPOSL) and nested (NESTPOSMAPOSL) linear Patlak 4D methods as well as for the non-linear generalized Patlak non-nested (GPOSMAPOSL) and nested (NESTGPOSMAPOSL) 4D reconstruction algorithms.

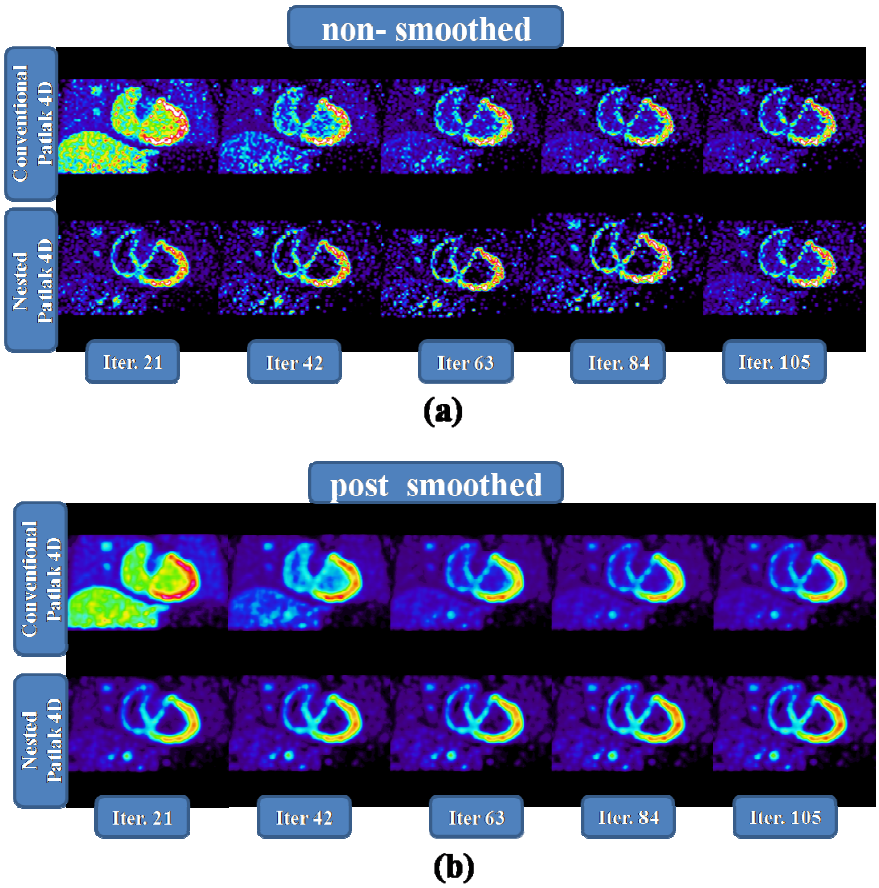

Figure 3. Comparative evaluation of nested vs. conventional direct 4D Patlak reconstructon in terms of (a) non-smoothed, as well as (b) post smoothed (Gaussian, FWHM=2mm) K_i parametric images (simulated data).

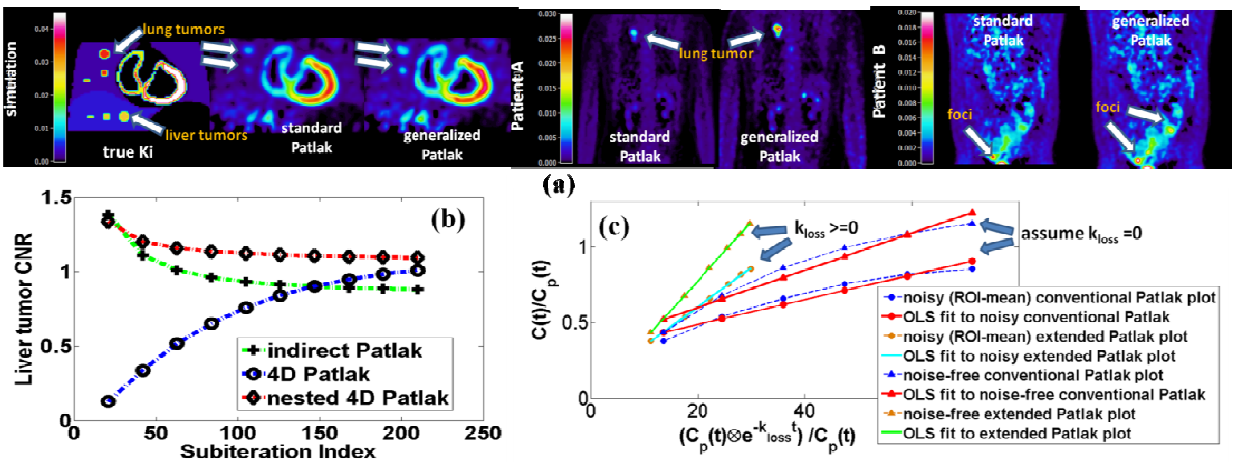

Figure 4 (a) Simulated true and estimated Ki images as well as clinical patient demonstration of standard vs. generalized Patlak models performance with indirect methos, (3b) Liver tumor CNR vs sub-iterations and (3c) Clinical patient demonstration of generalized Patlak imaging.

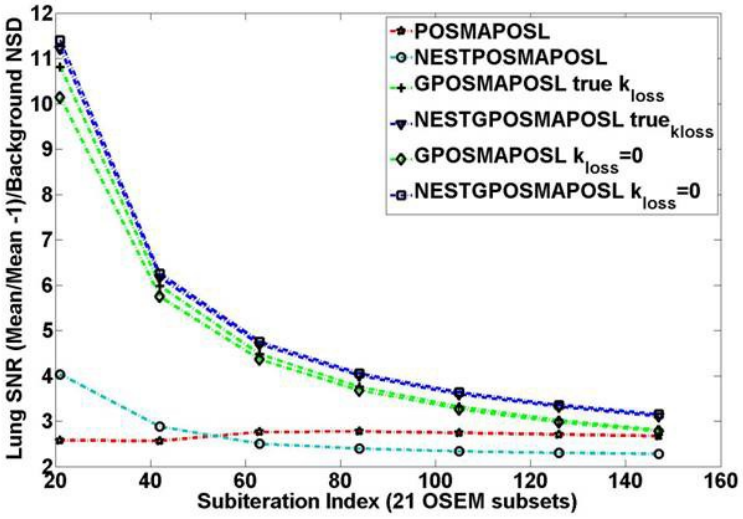

Figure 5. The SNR for the lung region of parametric K_i images against the number of iterations for a range of direct 4D Patlak reconstruction algorithms:

a) POSMAPOSL: linear standard Patlak direct 4D reconstruction, non-nested algorithm, equivalent to 1 nested loop at each iteration
b) NESTPOSMAPOSL: linear direct 4D reconstruction, optimization transfer/nested algorithm, 20 nested loops at each iteration
c) GPOSMAPOSL: non-linear generalized Patlak reconstruction, non-nested, equivalent to one nested loop at each iteration
d) NESTGPOSMAPOSL: non-linear generalized Patlak reconstruction, optimization transfer/nested algorithm, 7 nested loops at each iteration
e) true k_{loss}: algorithm initialized with true k_{loss} image
f) k_{loss}=0: algorithm initialized with k_{loss}=0 image

In all cases, the algorithms have been initialized with unity images for K_i and V parameters.

Furthermore, we evaluated the effect of the different initializations of the k_{loss} image for the generalized Patlak algorithms. The plots evidently suggest similarly superior SNR performance for both the GPOSMAPOSL and NESTGPOSMAPOSL methods with the latter consistently achieving the highest SNR in all iterations. The advantage of the generalized Patlak 4D reconstructions is evident for a wide range of moderate number of ML-EM iterations (21-100 iterations, 1 subset) and becomes smaller as the iterations further increase due to the ML-EM induced effect of amplification of noise at higher iteration numbers in the parametric images of all algorithms.

Moreover, the initialization of both generalized Patlak 4D algorithms with a standard zero k_{loss} image does not appear to affect their performance suggesting good convergence properties when k_{loss}=0 is used as initial estimate regardless of the true k_{loss} distribution. That was not the case when k_{loss}=1 which is a value likely to be very distant from the true especially when the units of k-values are proportional to sec^{-1}. Therefore, we recommend the following initialization as a standard for this type of algorithms: K_i=1, k_{loss}=0 and V=1.

The presented results are in agreement with what would be expected from the theory of section 2. Indeed, the incorporation of the generalized, as opposed to the standard, Patlak model within the 4D reconstruction (paragraph 2.4) is likely to further enhance the image quality of the parametric images in terms of SNR by a) potentially reducing the bias induced by the incomplete modeling of the standard Patlak and, at the same time, b) by suppressing the noise levels thanks to the better noise handling properties of the direct 4D reconstruction frameworks as elaborated in paragraph 1.1.

On the other hand, the computation time of the reconstruction increases considerably (~2-3 times depending on the

accuracy, i.e. number of time samples, in the convolution operations at each iteration, eq. 7) for the non-linear Patlak model. Moreover, the nested part of each iteration is no longer computationally faster than the rest of the processes of the iteration. Therefore, less number of nested loops must be applied for generalized Patlak schemes (7 compared to 20 used for standard Patlak), resulting in minor improvements in the convergence rate of the algorithm. Therefore, we recommend performing only a few (<7) nested updates per iteration for the generalized Patlak algorithms. At this point we should remind that the application of a single nested loop is equivalent to applying the respective non-nested version of the algorithms, as expected from theory and as we have confirmed after implementation.

5. CONCLUSIONS

In this study we designed and implemented in the STIR open source tomographic image reconstruction software a set of direct 4D Patlak reconstruction algorithms for both single-bed and whole-body dynamic PET studies. We conducted realistic dynamic simulations to validate our methods and quantitatively compared their performance in terms of CNR or SNR metrics.

First of all, our results demonstrate the importance of the introduction of the more complete generalized Patlak kinetic model as an alternative to the linear standard Patlak model through the quantitative evaluation of indirect parametric imaging performed both on simulated and clinical data. The new model significantly reduces bias but is not very robust to noise in the case of indirect parameter estimation due to its non-linear nature.

Furthermore, we present the potential benefits of incorporating the generalized Patlak model into a whole body direct 4D parametric image reconstruction framework to further enhance the image quality of the parametric images in terms of SNR by efficiently suppressing the noise. Indeed, our results suggest significant enhancement in the measured SNR of the parametric images, but the computational cost also increases considerably. In addition, a standardized initialization scheme is proposed to help avoid lack of or slowness in convergence.

Finally, the effect of the application of the optimization transfer principle in the standard and generalized Patlak ML-EM 4D reconstruction algorithms is evaluated. The resulting nested versions of the 4D algorithms converge faster than the non-nested algorithms and thus can be considered more clinically feasible, attractive and practical. However, the observed convergence acceleration is significant mainly for the linear standard Patlak 4D algorithm, while it is found to be considerably smaller for the non-linear algorithm.

ACKNOWLEDGMENTS

The authors would like to thank Dr. Kris Thielemans and Dr. Charalampos Tsoumpas for the guidance they provided regarding the usage of the basic STIR package. This work was in part supported by the NIH grant 1S10RR023623.

REFERENCES

[1] Wahl, R.L. and Buchanan, J.W., "Principles and Practice of Positron Emission Tomography," Lippincott Williams & Wilkins (2002)
[2] Karakatsanis, N.A. Lodge, M.A., Tahari, A.K., Zhou, Y., Wahl, R.L. and Rahmim, A., "Dynamic whole-body PET parametric imaging: I. Concept, acquisition protocol optimization and clinical application," Phys. Med. Bio., 58, p7391 (2013)
[3] Karakatsanis, N.A., Lodge, M.A., Zhou, Y., Wahl, R.L. and Rahmim, A., "Dynamic whole-body PET parametric imaging: II. Task-oriented statistical estimation," Phys. Med. Biol., 58, p. 7419 (2013)
[4] Patlak, C.S. and Blasberg, R.G., "Graphical evaluation of blood-to-brain transfer constants from multiple-time uptake data. Generalizations," J Cereb Blood Flow Metab, 5, p.584 (1985)

[5] Rahmim, A., Tang, J. and Zaidi, H., "Four-dimensional (4D) image reconstruction strategies in dynamic PET: Beyond conventional independent frame reconstruction," Med Phys, 36 (8), p.3654 (2009)
[6] Wang, G, Fu, L. and Qi, J., "Maximum a posteriori reconstruction of the Patlak parametric image from sinograms in dynamic PET," Phys Med Biol, vol. 53 (3) p. 593 (2008)
[7] Thielemans, K., Tsoumpas C., Mustafovic S., Beisel T., Aguiar P., Dikaios N. and Jacobson M.W., "STIR: software for tomographic image reconstruction release 2, " Phys Med Biol, vol. 57(4) (2012).
[8] Karakatsanis, N.A., Lodge, M.A., Wahl, R.L. and Rahmim, A., "Direct 4D whole-body PET/CT parametric image reconstruction: Concept and comparison vs. indirect parametric imaging," J Nucl Med, 54 (2013)
[9] Tsoumpas, C., Turkheimer, F.E. and Thielemans, K., "Study of direct and indirect parametric estimation methods of linear models in dynamic positron emission tomography," Med Phys, 35(4) (2008)
[10] Tsoumpas, C., Turkheimer, F.E. and Thielemans, K., "A survey of approaches for direct parametric image reconstruction in emission tomography," Med Phys, 35(9) (2008)
[11] Dimitrakopoulou-Strauss, A, Georgoulias, V., Eisenhut, M., Herth, F., Koukouraki, S., Macke, H., Haberkorn, U. and Strauss, L., "Quantitative assessment of SSTR2 expression in patients with non-small cell lung cancer using 68 Ga-DOTATOC PET and comparison with 18 F-FDG PET,", Eur J Nucl. Med. and Mol. Imaging, 33(7), p. 823–830 (2006)
[12] Okazumi, S., Dimitrakopoulou-Strauss, A., Schwarzbach, M.H. and Strauss, L.G., "Quantitative, dynamic 18F-FDGPET for the evaluation of soft tissue sarcomas: relation to differential diagnosis, tumor grading and prediction of prognosis," Hel. J. Nucl. Med., 12 (2009)
[13] Torizuka, T., Tamaki N., Inokuma T., Magata Y., Sasayama S., Yonekura Y., Tanaka A., Yamaoka Y. and Yamamoto K. and Konishi J., "In vivo assessment of glucose metabolism in hepatocellular carcinoma with FDG-PET," J. Nucl. Med., 36(10), p. 1811 (1995)
[14] Messa, C., Choi, Y., Hoh, C.K., Jacobs, E.L., Glaspy, J.A., Rege, S., Nitzsche E., Huang, S.C., Phelps, M.E. and Hawkins, R.A., "Quantification of glucose utilization in liver metastases: parametric imaging of FDG uptake with PET," J Comput Assist Tomogr,16(5), p. 684-9 (1992)
[15] Sayre, G.A., Franc, B.L. and Seo, Y., "Patient-Specific Method of Generating Parametric Maps of Patlak Ki without Blood Sampling or Metabolite Correction: A Feasibility Study," Int J Mol Imaging, Art. ID 185083 (2011)
[16] Hoh, C., Vera, D. and Schiepers, C., "Reducing effects of non-zero k4 and metabolites in generating Patlak parametric images of FLT uptake," J Nucl Med, 52, p. 2063 (2011)
[17] Wang, G., and Qi, J., "Acceleration of the direct reconstruction of linear parametric images using nested algorithms, " Phys Med Biol, 55(5), p. 1505 (2010)
[18] Wang, G., and Qi, J., "Direct estimation of kinetic parametric images for dynamic PET," Theranostics, (2013)
[19] Yan, J., Planeta-Wilson, B., and Carson, R.E., "Direct 4-D PET List Mode Parametric Reconstruction With a Novel EM Algorithm," IEEE Trans Med Imaging, 31(12), p. 2213 (2012)
[20] Gunn, R.N., Lammertsma A.A., Hume S.P. and Cunningham V.J., "Parametric imaging of ligand-receptor binding in PET using a simplified reference region model," Neuroimage, 6(4), p. 279 (1997)